Published in final edited form as:
FEBS Lett. 2009 November 3; 583(21): 3467–3472. doi:10.1016/j.febslet.2009.09.050.

Two-dimensional Pulsed Electron Spin Resonance Characterization of ^{15}N-Labeled Archaeal Rieske-type Ferredoxin

Toshio Iwasaki[*,a], **Rimma I. Samoilova**[b], **Asako Kounosu**[a], and **Sergei A. Dikanov**[*,c]

[a] Department of Biochemistry and Molecular Biology, Nippon Medical School, Sendagi, Tokyo 113-8602, Japan

[b] Institute of Chemical Kinetics and Combustion, Russian Academy of Sciences, Novosibirsk 630090, Russia

[c] Department of Veterinary Clinical Medicine, University of Illinois at Urbana-Champaign, Urbana, Illinois 61801, U.S.A

Abstract

Two-dimensional electron spin-echo envelope modulation (HYSCORE) analysis of the uniformly ^{15}N-labeled archaeal Rieske-type [2Fe-2S] ferredoxin (ARF) from *Sulfolobus solfataricus* P1 has been conducted in comparison with the previously characterized high-potential protein homologs. Major differences among these proteins were found in the HYSCORE lineshapes and intensities of the signals in the (++) quadrant, which are contributed from weakly coupled (non-coordinated) peptide nitrogens near the reduced clusters. They are less pronounced in the HYSCORE spectra of ARF than those of the high-potential protein homologs, and may account for the tuning of Rieske-type clusters in various redox systems.

Keywords

EPR; ESEEM; HYSCORE; Rieske; ferredoxin; [2Fe-2S] cluster; archaea

1. Introduction

Proteins containing Rieske-type [2Fe-2S](His)$_2$(Cys)$_2$ clusters are involved in a wide range of biological electron transfer reactions such as aerobic respiration, photosynthesis, and biodegradation of various alkene and aromatic compounds [1–6]. Rieske proteins from quinol-oxidizing cytochrome bc_1/b_6f complexes contain a high-potential [2Fe-2S] cluster (with midpoint redox potential (E_m) of ~+150 to +490 mV), whereas the archaeal and bacterial Rieske-type ferredoxins have a relatively low-potential cluster (~−150 to −50 mV). The available crystallographic structures indicate that these proteins are structurally related and that a lower potential cluster tends to have less extensive hydrogen bonding network around the cluster [7–9]. The combined density functional theory/continuum electrostatics analysis further suggests a contribution of negatively charged residues in the low-potential homolog [10]. Thus, versatility of the cluster E_m's might have been achieved in the modular evolution of the cluster binding domain by accumulative natural mutations of the local non-coordinated residues around the tuneable cluster.

*Corresponding authors. Fax: 81-3-5685-3054. tiwasaki@nms.ac.jp (T. Iwasaki), Fax: 217-333-8868. dikanov@illinois.edu (S. A. Dikanov).

Pulsed electron paramagnetic resonance (EPR) techniques such as electron spin-echo envelope modulation (ESEEM) and electron-nuclear double resonance (ENDOR) probe coupling between electron and nuclear spins, and have become popular tools in the detailed analyses of various proteins with paramagnetic centers, often aided by isotopic labeling and other physicochemical methods [11–14]. The tuneable [2Fe-2S] cluster in Rieske-type proteins is hydrogen bonded with multiple backbone peptide nitrogens (N_p's) [7–9], some of which can be potentially resolved and quantitatively analyzed by the ESEEM measurement of the hyperfine (HF) frequencies of nuclei (such as ^{1}H, ^{2}H, ^{14}N, and ^{15}N) that interact with the effective S=1/2 electron spin of the reduced cluster.

In our previous study, we have established the heterologous overexpression system in *Escherichia coli* for two hyperthermophile Rieske-type protein homologs with the specific aim of exploring the differences in their cluster environments: (i) an archaeal low-potential Rieske-type ferredoxin (ARF) from *Sulfolobus solfataricus* strain P1 ($E_{m,7}$ ~−60 mV) with homology to oxygenase-associated Rieske-type ferredoxins (DDBJ-EMBL-GenBank code, AB047031) and (ii) an archaeal high-potential Rieske protein called sulredoxin (SDX) from *Sulfolobus tokodaii* strain 7 ($E_{m,acid\ pH}$ ~+190 mV) with weak homology to cytochrome *bc*-associated Rieske proteins (DDBJ-EMBL-GenBank code, AB023295) [15–18]. Particular effort was devoted to analyzing the comparative, two-dimensional four-pulse ESEEM (also called hyperfine sublevel correlation, HYSCORE) spectra of ^{14}N(natural abundance, N/A)-ARF and SDX, which have shown two major factors affecting the spectral differences from the "strongly coupled (coordinated)" $^{14}N_\delta$ of histidine ligands [17]: (i) the variation of the N_δ *quadrupole couplings* that are influenced by the changes in coordination geometry of histidine imidazole ligands to the reduced cluster, and (ii) the variation of the N_δ *HF couplings* that are affected to a lesser degree by the changes of the ligand geometry and the differences in the polypeptide environment. Additionally, we suggested a possible different interaction of the reduced cluster with certain backbone N_p's in these proteins [17]. However, the powder-type ^{14}N HYSCORE spectra provided limited information about the "weakly coupled (non-coordinated)" remote N_ε (of the histidine ligands) and N_p's, due to the influence of nuclear quadrupole interaction requiring special relations between the nuclear Zeeman frequency and HF coupling [19]. These weakly coupled nitrogens can be better resolved by the orientation-selected HYSCORE analysis of ^{15}N-labeled proteins, because ^{15}N does not contain the quadrupole moment. Currently, ^{15}N HYSCORE characterization is available only for the high-potential Rieske proteins [18,20,21], although several ^{14}N studies have been reported for the low-potential homologs with emphasis on the strong couplings from histidine N_δ ligands [17,22–24].

Here we report the ^{15}N HYSCORE investigation of a low-potential Rieske-type ferredoxin for the first time, characterizing the coordinated and non-coordinated nitrogen nuclei around the reduced [2Fe-2S] cluster in the uniformly ^{15}N-labeled ARF (^{15}N-ARF). We discuss the similarities and variations of ^{15}N HYSCORE features among different types of the Rieske protein family.

2. Experimental procedures

2.1. Materials and sample preparation

Escherichia coli strain JM109 (TaKaRa, Japan) used for cloning was grown in Lauria-Bertani (LB) medium, with 50 μg/ml kanamycin when required. Water was purified by a Millipore Milli-Q purification system. Other chemicals mentioned in this study were of analytical grade.

The uniformly ^{15}N-labeled, recombinant ARF (DDBJ-EMBL-GenBank code, AB047031) from the hyperthermoacidophilic archaeon *Sulfolobus solfataricus* P1 was prepared as reported previously, using the combinations of the pTrc99A vector (Amersham Biosciences)/*E. coli* CodonPlus(DE3)-RIL host strain (Stratagene)/M9 salt-based synthetic medium system [15].

2.2. ESEEM and HYSCORE analyses

X-band pulsed EPR measurements were carried out by using an X-band Bruker ELEXSYS E580 spectrometer with an Oxford CF 935 cryostat at 10–11 K. ESEEM experiments with two-pulse and two-dimensional four-pulse sequences were employed, with appropriate phase cycling schemes to eliminate unwanted features from experimental echo envelopes, as previously described in detail [17]. Spectral processing of ESEEM patterns, including subtraction of relaxation decay (fitting by polynoms of 3–6 deg), apodization (Hamming window), zero filling, and fast Fourier transformation (FT), was performed using Bruker WIN-EPR software.

3. Results and discussion

3.1. Strongly coupled (coordinated) $^{15}N_{\delta}1,2$ in the (+−) quadrant of the HYSCORE spectra

Strong antiferromagnetic coupling between the electron spins of two irons of the biological [2Fe-2S] cluster produces an EPR-silent (S=0) ground state in the oxidized Fe^{3+}-Fe^{3+} form and a paramagnetic S=1/2 ground state in the reduced Fe^{3+}-Fe^{2+} form. Dithionite-reduced Rieske-type [2Fe-2S] cluster in ARF is characterized by the anisotropic EPR spectrum, as a result of a rhombic g-tensor ($g_{z,y,x}$=2.02, 1.90, 1.81) [15]. The two-dimensional HYSCORE spectrum consists of non-diagonal cross-peaks, whose coordinates are nuclear frequencies from electron spin m_s=+1/2 and −1/2 manifolds belonging to the same nucleus [11]. Because ^{15}N with nuclear spin I=1/2 has only two nuclear frequencies, each ^{15}N may produce only a single pair of the cross-features which are located symmetrically relative to the diagonal line in the (+−) or (++) quadrant of the HYSCORE spectrum (depending on the ^{15}N HF coupling strength). The cross-features produced by different types of ^{15}N could be successfully resolved in the orientation-selected HYSCORE spectra of ^{15}N-ARF measured at different points of the EPR line (Fig. 1A,B). In the (+−) quadrant, two pairs of cross-peaks with a contour parallel to the diagonal line are detected, which are attributed to the two coordinated histidine $^{15}N_{\delta}1,2$ to the reduced cluster with the HF couplings of the order 6 and 8 MHz. As shown in Fig. 1C, the frequency coordinates of the data points from the cross-peaks in the (+−) quadrant were measured across the entire EPR line at different external magnetic field positions, and then plotted in the coordinates $(\nu_1)^2$-*versus*-$(\nu_2)^2$ after recalculating their frequencies for a common ν_I=1.511 MHz [25,26]. In this representation, all data points fell along two straight lines, described by the following equation:

$$\nu_1^2 = Q\nu_2^2 + G$$

where $Q = \frac{T + 2a - 4\nu_I}{T + 2a + 4\nu_I}$ and $G = \frac{2\nu_I(4\nu_I^2 - a^2 + 2T^2 - aT)}{T + 2a + 4\nu_I}$.

The slope and intercept of each line from the linear regression fit determine the isotropic and anisotropic parts of the HF tensors (in the axial approximation) for each strongly coupled (coordinated) $^{15}N_{\delta}$ ($^{15}N_{\delta}1$, open circle; $^{15}N_{\delta}2$, filled circle) of ^{15}N-ARF (Fig. 1C and Table 1). These values are very similar to those reported for other Rieske-type proteins by the orientation-selected ^{15}N HYSCORE [18,20,21] (Table 1) and ^{15}N Q-band ENDOR [27]. On the basis of the previous ^{14}N HYSCORE analyses of *Rhodobacter sphaeroides* cytochrome bc_1 complex [28] and ^{14}N(N/A)-ARF and SDX [17], two strong couplings $^{15}N_{\delta}1$ and $^{15}N_{\delta}2$ were tentatively assigned as the His44N_{δ} and His64N_{δ} ligands, respectively, of ARF (Table 1). One of these ligand residues, His64, can be substituted by cysteine to accommodate a fairly stable, oxidized [2Fe-2S](Cys)$_3$(His)$_1$ cluster in the ARF scaffold [15].

3.2. Weakly coupled $^{15}N_{\varepsilon}$ in the (++) quadrant of the HYSCORE spectra

The (++) quadrant of the ^{15}N-ARF spectra contains features centered symmetrically around the diagonal point with ^{15}N Zeeman frequency and attributed to weakly coupled (non-coordinating) ^{15}N nuclei near the reduced cluster (Fig. 1A,B). These features were best resolved in the "single-crystal-like" HYSCORE spectra recorded at the low- and high-field edges near the maximal and minimal g values (Fig. 2A,B,D). Near the g_z area (low-field edge), two superimposed but relatively well-resolved pairs of the cross-features are detected at [2.01; 0.98] MHz ($^{15}N_p$) and [1.71; 1.28] MHz ($^{15}N_{\varepsilon}$), with the splittings of 1.03 and 0.43 MHz, respectively (Figs. 1A, 2A). Near the g_x area (high-field edge), they are at [2.23; 1.13] MHz ($^{15}N_p$) and [1.92; 1.43] MHz ($^{15}N_{\varepsilon}$), with the splittings of 1.1 and 0.49 MHz, respectively (Fig. 2D). The similar splittings were also observed at some intermediate positions between the low- and high-field edges (*e.g.*, see Figs. 1B, 2C), indicating their predominantly isotropic characters. This HYSCORE spectral pattern (but with small variations in their values) is reminiscent of those reported for the high-potential Rieske protein homologs [18,20,21] (Table 1).

The isotropic HF coupling of the directly coordinated N_{δ} of the imidazole ring to a paramagnetic metal center is about 20 times larger than that of the (non-coordinated) remote N_{ε} in various model complexes and metalloproteins [14,29]. This property is probably owing to the analogous spin density transfer phenomenon from the metal ion over the imidazole ring to the remote N_{ε}, which is also sensitive to the protonation state of the N_{ε} [14,29]. Thus, the intense pair of the cross-features with the smaller splitting of ~0.3–0.5 MHz in the HYSCORE spectra of these proteins (*e.g.*, N_{ε} in Fig. 2A) are consistent with those from the protonated form of the remote N_{ε}'s of two histidine ligands to the reduced cluster (Table 1). The nuclear magnetic resonance (NMR) assignments of the HF-shifted resonances for His47N_{ε} and His64N_{ε} of a closely related Rieske-type ferredoxin component (T4moC) of the *Pseudomonas mendocina* toluene 4-monooxygenase complex [30,31] suggest that the two $^{15}N_{\varepsilon}$ nuclei of ARF are expected to have very similar HF couplings. They probably remain unresolved in the ^{15}N X-band HYSCORE spectra where the estimated difference is comparable with the individual spectral line-widths.

3.3. Variations of other weakly coupled nitrogens among Rieske-type proteins

The (N/O)-H···S hydrogen bond network around the biological iron-sulfur clusters is one of the most important themes in modulating their redox properties. In the case with the N-H···S hydrogen bonds with the bridging and terminal sulfur atoms of the reduced iron-sulfur cluster system, the *s*- and *p*-orbitals of the nitrogens carry unpaired spin density transferred from the reduced cluster through chemical bonds (including hydrogen bonds). These spin densities can be observable as HF couplings in the ESEEM spectra [18–21,32].

In the (++) quadrant of the ^{15}N-ARF spectra, the largest HF coupling of ~1.1 MHz is clearly resolved (Fig. 2), which is comparable to those previously detected in the ESEEM spectra of the plant and vertebrate [2Fe-2S](Cys)$_4$ ferredoxins (~0.7 and ~1.1 MHz for $^{14}N_p$, or ~1 and ~1.5 MHz for $^{15}N_p$, respectively) [32] and the high-potential Rieske protein homologs (~1.1 MHz for $^{15}N_p$) [18,20,21] (Table 1). The equivalent HF coupling ~1.1 MHz in the ^{15}N HYSCORE spectra of the *R. sphaeroides* high-potential Rieske protein has been determined to come from Leu132N_{α} [21]. Notably, the NMR analysis of T4moC, which is closely related to ARF, showed the maximal chemical shift of ~426 ppm for the HF-shifted Gln48$^{15}N_{\alpha}$ (equivalent to Lys45N_{α} in ARF [DDBJ-EMBL-GenBank code, AB047031] and Leu132N_{α} in the *R. sphaeroides* Rieske protein [21]) in the reduced protein (with the largest change of chemical shift by ~300 ppm upon reduction of the cluster) [30,31]. In the 1.48-Å structure of the Cys84Ala/Cys85Ala double mutant of T4moC (1vm9.pdb), this N_p is hydrogen-bonded with the bridging sulfide S1 of the [2Fe-2S] cluster (Gln48N_{α}-S1 distance, 3.4 Å) [33]. Based

on these considerations, we tentatively assigned the largest HF coupling of ~1.1 MHz in the (++) quadrant of the HYSCORE spectra to the $^{15}N_p$ nucleus (presumably Lys45N_α) of ARF (Fig. 2), which holds some unpaired spin density transferred from the reduced Rieske-type cluster via the N-H¨¨S hydrogen bonding. In retrospect, the previously observed cross-features **P_1** and **P_2** in the ^{14}N(N/A)-ARF spectra [17] can be re-assigned as the double quantum-double quantum (dq-dq) and double quantum-single quantum (dq-sq) features, respectively, of the same N_p nucleus with the coupling ~1.1 MHz (for ^{15}N).

The NMR analysis of T4moC also showed the presence of other HF-shifted N_p's, such as Ala66N_α (equivalent to Leu63N_α in ARF [DDBJ-EMBL-GenBank code, AB047031]) which is hydrogen bonded with the terminal Cys64S_γ ligand [30,31]. In principle, the ^{15}N HYSCORE spectra can potentially provide information about all nitrogens involved in the *measurable* magnetic interactions with the unpaired electron spin of the reduced cluster, contrary to the ^{14}N HYSCORE spectra. The $^{15}N_\delta$1,2 couplings giving cross-peaks in the (+−) quadrant of the spectra (Fig. 2A) vary only slightly among different Rieske-type proteins (Table 1), suggesting that they should produce small changes in the corresponding relative intensities under the same experimental settings. The relative cross-peak intensities contributed from two $^{15}N_\delta$ ligands in the (+−) quadrant were therefore normalized after re-scaling and used as the internal references for the comparison of the spectral intensities of the aggregate $^{15}N_\varepsilon/^{15}N_p$ peaks in the (++) quadrant. Close inspection of the resulting ^{15}N HYSCORE spectra of different Rieske-type proteins indicates the substantial variations in the lineshapes and relative intensities of their doublet components and the area around the diagonal point, in the (++) quadrant (Fig. 2B–D). Thus, although the present ^{15}N-ARF spectra have apparently resolved the remote $^{15}N_\varepsilon$ and the largest $^{15}N_p$ couplings with the splittings 0.3–0.5 and ~1.1 MHz, respectively, like those reported for the high-potential protein homologs [18, 20,21] (Table 1), these variations clearly indicate additional contributions of non-equivalent weak HF couplings from other ^{15}N nuclei to the ESEEM amplitude in this particular region. Their possible candidates may be $^{15}N_p$(s) of other non-coordinating residues around the reduced cluster and the terminal cyteine ligands, most of which should not give resolved cross-peaks in the corresponding ^{14}N HYSCORE spectra [17,22–24]. This is important, because the overlap of these additional signals (weak couplings with narrow lineshapes), especially in the cases of the high-potential protein homologs, would interfere with the $^{15}N_\varepsilon$ splitting that is currently measured directly from the cross-peak positions (Fig. 2B–D). Because the ESEEM amplitudes are complicated functions of spin Hamiltonian operator parameters and experimental settings [11,12], deconvoluting each of these signals is practically difficult. Their further resolution and assignments would therefore require extensive site-specific isotope labeling of the residues near the cluster.

4. Concluding remarks

The HF couplings of the remote N_ε of the histidine ligands to the reduced Rieske-type [2Fe-2S] cluster give only weak peaks that are masked by those from weakly coupled N_p's in ESEEM spectra. The best way to detect these nuclei with the X-band experiments for the future functional study is through substitution of ^{14}N by ^{15}N. The ^{15}N HYSCORE characterization of dithionite-reduced ^{15}N-ARF provides the first resolution of $^{15}N_\varepsilon$ and one of $^{15}N_p$ nuclei in a low-potential Rieske-type ferredoxin, which gave very similar HF couplings as those reported for the high-potential protein homologs [18,20,21] (Table 1). These features probably reflect the common structural framework and physical nature of the biological iron-sulfur clusters of this functionally versatile class, regardless of the cluster E_m's.

Significant variations were found among different Rieske-type proteins in the (++) quadrant of the corresponding, orientation-selected ^{15}N HYSCORE spectra, where the weak HF couplings with narrow lineshapes from other $^{15}N_p$'s appear to overlap with the $^{15}N_\varepsilon$ splitting

and may interfere with its cross-peak positions. These weak couplings are less pronounced (but also present) in the ^{15}N-ARF spectrum, indicating less contribution from these extra non-coordinated (probably peptide) nitrogens in the reduced ARF cluster system.

Acknowledgments

This work was supported in part by JSPS Grants-in-aid 15770088, 18608004 and 21659111 (T.I.), by JSPS Grant BSAR-507 (T.I.), by NSF Grant 9910113 (S.A.D.), and by NIH Grant GM62954 (S.A.D.).

Abbreviations

ARF	archaeal Rieske-type ferredoxin from *Sulfolobus solfataricus*
ENDOR	electron nuclear double resonance
EPR	electron paramagnetic resonance
ESEEM	electron spin-echo envelope modulation
FT	Fourier transform
E_m	redox potential
HF	hyperfine
HYSCORE	hyperfine sublevel correlation
NMR	nuclear magnetic resonance
N_p	peptide backbone nitrogen
SDX	sulredoxin (a high-potential Rieske protein from *Sulfolobus tokodaii*)
T4moC	Rieske-type ferredoxin component of toluene 4-monooxygenase complex

References

1. Mason JR, Cammack R. The electron-transport proteins of hydroxylating bacterial dioxygenases. Annu Rev Microbiol 1992;46:277–305. [PubMed: 1444257]
2. Trumpower BL, Gennis RB. Energy transduction by cytochrome complexes in mitochondrial and bacterial respiration: the enzymology of coupling electron transfer reactions to transmembrane proton translocation. Annu Rev Biochem 1994;63:675–716. [PubMed: 7979252]
3. Link TA. The structures of Rieske and Rieske-type proteins. Adv Inorg Chem 1999;47:83–157.
4. Berry EA, Guergova-Kuras M, Huang LS, Crofts AR. Structure and function of cytochrome *bc* complexes. Annu Rev Biochem 2000;69:1005–1075. [PubMed: 10966481]
5. Crofts AR. The cytochrome bc_1 complex: function in the context of structure. Annu Rev Physiol 2004;66:689–733. [PubMed: 14977419]
6. Cramer WA, Zhang H, Yan J, Kurisu G, Smith JL. Transmembrane traffic in the cytochrome b_6f complex. Annu Rev Biochem 2006;75:769–790. [PubMed: 16756511]
7. Iwata S, Saynovits M, Link TA, Michel H. Structure of a water soluble fragment of the 'Rieske' iron-sulfur protein of the bovine heart mitochondrial cytochrome bc_1 complex determined by MAD phasing at 1.5 Å resolution. Structure 1996;4:567–579. [PubMed: 8736555]
8. Colbert CL, Couture MMJ, Eltis LD, Bolin J. A cluster exposed: structure of the Rieske ferredoxin from biphenyl dioxygenase and redox properties of Rieske Fe-S proteins. Structure 2000;8:1267–1278. [PubMed: 11188691]
9. Hunsicker-Wang LM, Heine A, Chen Y, Luna EP, Todaro T, Zhang YM, Williams PA, McRee DE, Hirst J, Stout CD, Fee JA. High-resolution structure of the soluble, respiratory-type Rieske protein

from *Thermus thermophilus*: analysis and comparison. Biochemistry 2003;42:7303–7317. [PubMed: 12809486]

10. Klingen AR, Ullmann GM. Negatively charged residues and hydrogen bonds tune the ligand histidine pK_a values of Rieske iron-sulfur proteins. Biochemistry 2004;43:12383–12389. [PubMed: 15449929]
11. Dikanov, SA. Two-dimensional ESEEM spectroscopy. In: Atta-ur-Rahman, editor. New Advances in Analytical Chemistry. Gordon and Breach; Amsterdam: 2000. p. 523-568.
12. Prisner T, Rohrer M, MacMillan F. Pulsed EPR spectroscopy: biological applications. Annu Rev Phys Chem 2001;52:279–313. [PubMed: 11326067]
13. Hoffman BM. Electron-nuclear double resonance spectroscopy (and electron spin-echo envelope modulation spectroscopy) in bioinorganic chemistry. Proc Natl Acad Sci USA 2003;100:3575–35778. [PubMed: 12642664]
14. Mims, WB.; Peisach, J. ESEEM and LEFE of metalloproteins and model compounds. In: Hoff, AJ., editor. Advanced EPR: Applications in Biology and Biochemistry. Elsevier; Amsterdam: 1989. p. 1-57.
15. Kounosu A, Li Z, Cosper NJ, Shokes JE, Scott RA, Imai T, Urushiyama A, Iwasaki T. Engineering a three-cysteine, one-histidine ligand environment into a new hyperthermophilic archaeal Rieske-type [2Fe-2S] ferredoxin from *Sulfolobus solfataricus*. J Biol Chem 2004;279:12519–12528. [PubMed: 14726526]
16. Iwasaki T, Kounosu A, Kolling DRJ, Crofts AR, Dikanov SA, Jin A, Imai T, Urushiyama A. Characterization of the pH-dependent resonance Raman transitions of archaeal and bacterial Rieske [2Fe-2S] proteins. J Am Chem Soc 2004;126:4788–4789. [PubMed: 15080677]
17. Dikanov SA, Shubin AA, Kounosu A, Iwasaki T, Samoilova RI. A comparative, two-dimensional ^{14}N ESEEM characterization of reduced [2Fe-2S] clusters in hyperthermophilic archaeal high- and low-potential Rieske-type proteins. J Biol Inorg Chem 2004;9:753–767. [PubMed: 15243789]
18. Iwasaki T, Kounosu A, Uzawa T, Samoilova RI, Dikanov SA. Orientation-selected ^{15}N-HYSCORE detection of weakly coupled nitrogens around the archaeal Rieske [2Fe-2S] center. J Am Chem Soc 2004;126:13902–13903. [PubMed: 15506733]
19. Dikanov SA, Tyryshkin AM, Felli I, Reijerse EJ, Hüttermann J. C-band ESEEM of strongly coupled peptide nitrogens in reduced two-iron ferredoxin. J Magn Reson, Ser B 1995;108:99–102. [PubMed: 7627437]
20. Iwasaki T, Kounosu A, Samoilova RI, Dikanov SA. ^{15}N HYSCORE characterization of the fully deprotonated, reduced form of the archaeal Rieske [2Fe-2S] center. J Am Chem Soc 2006;128:2170–2171. [PubMed: 16478144]
21. Dikanov SA, Kolling DRJ, Endeward B, Samoilova RI, Prisner TF, Nair SK, Crofts AR. Identification of hydrogen bonds to the Rieske cluster through the weakly coupled nitrogens detected by electron spin echo envelope modulation spectroscopy. J Biol Chem 2006;281:27416–27425. [PubMed: 16854984]
22. Shergill JK, Joannou CL, Mason JR, Cammack R. Coordination of the Rieske-type [2Fe-2S] cluster of the terminal iron-sulfur protein of *Pseudomonas putida* benzene 1,2-dioxygenase, studied by one- and two-dimensional electron spin-echo envelope modulation spectroscopy. Biochemistry 1995;34:16533–16542. [PubMed: 8527426]
23. Dikanov SA, Xun L, Karpiel AB, Tyryshkin AM, Bowman MK. Orientationally-selected two-dimensional ESEEM spectroscopy of the Rieske-type iron-sulfur cluster in 2,4,5-trichlorophenoxyacetate monooxygenase from *Burkholderia cepacia* AC1100. J Am Chem Soc 1996;118:8408–8416.
24. Dikanov SA, Davydov RM, Xun L, Bowman MK. CW and pulsed EPR characterization of the reduction of the Rieske-type iron sulfur cluster in 2,4,5-trichlorophenoxyacetate monooxygenase from *Burkholderia cepacia* AC1100. J Magn Reson Ser B 1996;112:289–294. [PubMed: 8812918]
25. Dikanov SA, Bowman MK. Determination of ligand conformation in reduced [2Fe-2S] ferredoxin from cysteine β-proton hyperfine couplings. J Biol Inorg Chem 1998;3:18–29.
26. Dikanov SA, Davydov RM, Gräslund A, Bowman MK. Two-dimensional ESEEM spectroscopy of nitrogen hyperfine couplings in methemerythrin and azidomethemerythrin. J Am Chem Soc 1998;120:6797–6805.

27. Gurbiel RJ, Doan PE, Gassner GT, Macke TJ, Case DA, Ohnishi T, Fee JA, Ballou DP, Hoffman BM. Active site structure of Rieske-type proteins: electron nuclear double resonance studies of isotopically labeled phthalate dioxygenase from *Pseudomonas cepacia* and Rieske protein from *Rhodobacter capsulatus* and molecular modeling studies of a Rieske center. Biochemistry 1996;35:7834–7845. [PubMed: 8672484]

28. Samoilova RI, Kolling D, Uzawa T, Iwasaki T, Crofts AR, Dikanov SA. The interaction of the Rieske iron-sulfur protein with occupants of the Q_o-site of the bc_1 complex, probed by electron spin echo envelope modulation. J Biol Chem 2002;277:4605–4608. [PubMed: 11748214]

29. Dikanov SA, Samoilova RI, Smieja JA, Bowman MK. Two-dimensional ESEEM study of VO^{2+} complexes with imidazole and histidine: histidine is a polydentante ligand. J Am Chem Soc 1995;117:10579–10580.

30. Xia B, Pikus JD, Xia W, McClay K, Steffan RJ, Chae YK, Westler WM, Markley JL, Fox BG. Detection and classification of hyperfine-shifted ^{1}H, ^{2}H, and ^{15}N resonances of the Rieske ferredoxin component of toluene 4-monooxygenase. Biochemistry 1999;38:727–739. [PubMed: 9888813]

31. Skjeldal L, Peterson FC, Doreleijers JF, Moe LA, Pikus JD, Westler WM, Markley JL, Volkman BF, Fox BG. Solution structure of T4moC, the Rieske ferredoxin component of the toluene 4-monooxygenase complex. J Biol Inorg Chem 2004;9:945–953. [PubMed: 15452777]

32. Dikanov SA, Samoilova RI, Kappl R, Crofts AR, Hüttermann J. The reduced [2Fe-2S] clusters in adrenodoxin and *Arthrospira platensis* ferredoxin share spin density with protein nitrogens, probed using 2D ESEEM. Phys Chem Chem Phys 2009;11:6807–6819. [PubMed: 19639155]

33. Moe LA, Bingman CA, Wesenberg GE, Phillips GNJ, Fox BG. Structure of T4moC, the Rieske-type ferredoxin component of toluene 4-monooxygenase. Acta Cryst Sect D 2006;62:476–482. [PubMed: 16627939]

34. Dikanov SA, Tyryshkin AM, Bowman MK. Intensity of cross-peaks in HYSCORE spectra of S = 1/2, I = 1/2 spin systems. J Magn Reson 2000;144:228–242. [PubMed: 10828191]

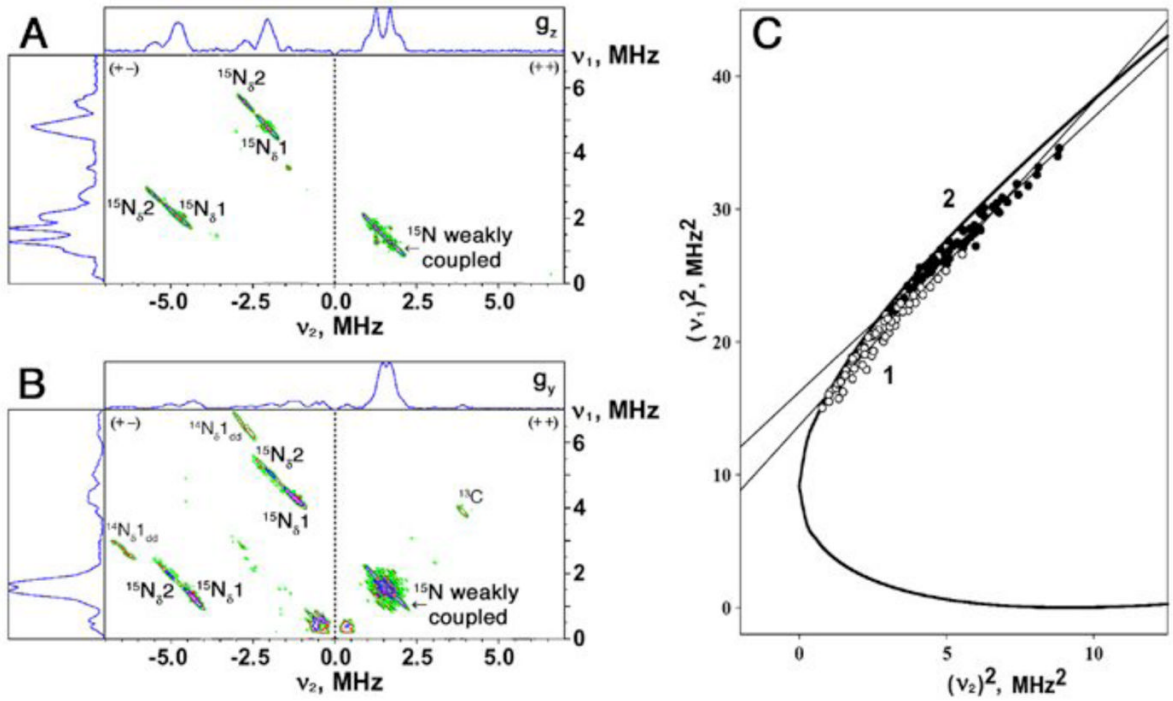

Fig. 1.

HYSCORE spectra in contour presentation of the reduced Rieske-type [2Fe-2S] cluster in the uniformly ^{15}N-labeled ARF, recorded at the g_z (A) and g_y (B) areas of the EPR line. The $(\nu_1)^2$-*versus*-$(\nu_2)^2$ plot for recalculated frequencies at a common ν_I=1.511 MHz (C) [25], where all data points for the cross-peaks correlating $^{15}N_\delta1$ (open circle) and $^{15}N_\delta2$ (filled circle), respectively, of ^{15}N-ARF fell along straight line with slope and intercept: Q1=2.44 (S.E. 0.07), G1=13.7 (S.E. 0.2) MHz^2 (for $^{15}N_\delta1$) and Q2=2.07 (S.E. 0.04), G2=16.2 (S.E. 0.2) MHz^2 (for $^{15}N_\delta2$). These parameters gave the anisotropic HF tensor ^{15}a=6.5 MHz, ^{15}T=1.5 MHz for $^{15}N_\delta1$, and ^{15}a=7.9 MHz, ^{15}T=1.6 MHz for $^{15}N_\delta2$ (see Table 1). The heavy curve (C) is defined by $|\nu_1+\nu_2|=2\nu_I$. Magnetic field, time τ, and microwave frequency, respectively: 342.5 mT (near g_z), 136 ns, 9.695 GHz (A); 363.1 mT (near g_y), 136 ns, 9.695 GHz (B).

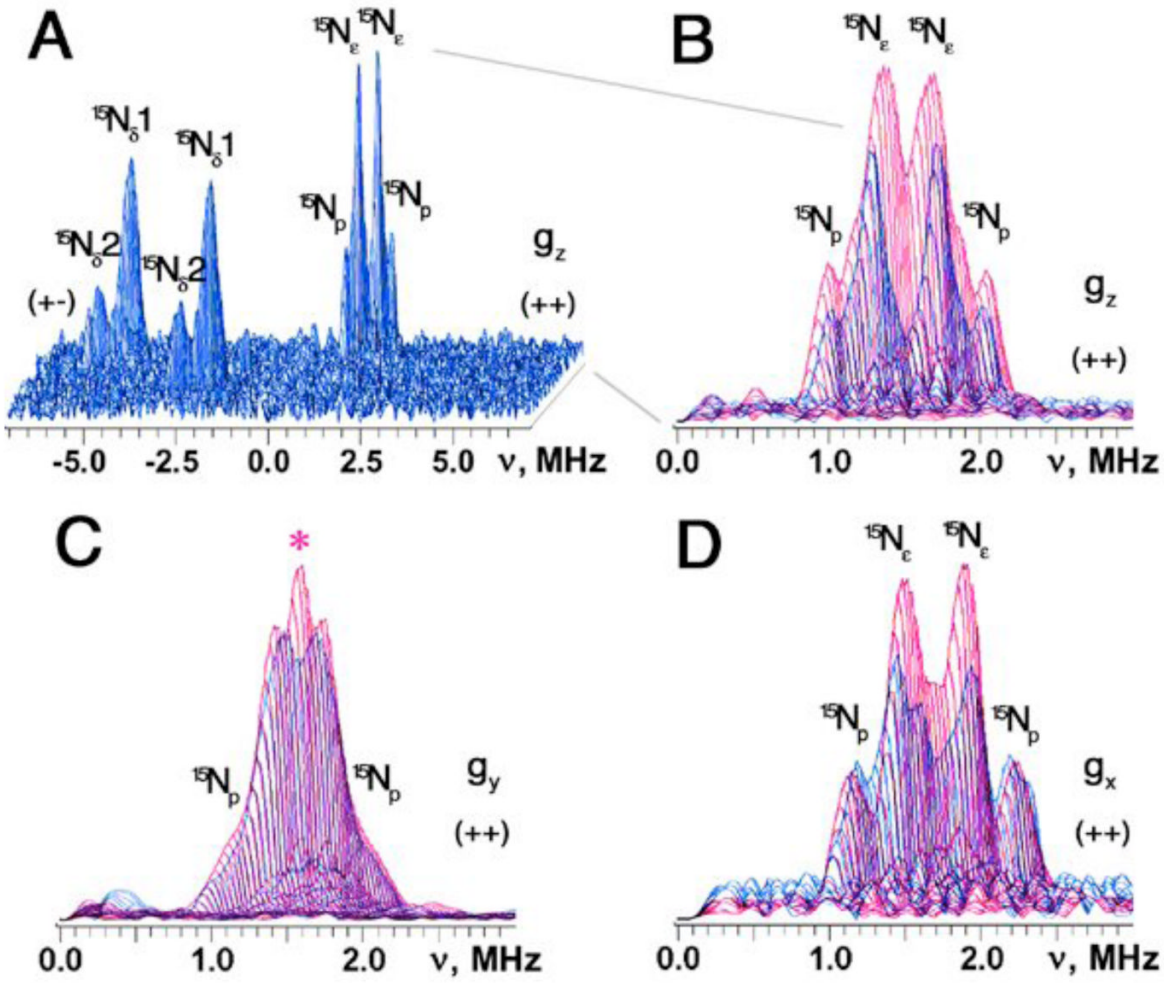

Fig. 2.

HYSCORE spectra in 3D presentation of the uniformly ^{15}N-labeled ARF recorded near the g_z area (A) and superimposed stacked HYSCORE spectra in the (++) quadrant of ^{15}N-ARF (blue) and ^{15}N-SDX (red), recorded near the g_z (B), g_y (C), and g_x (D) areas. At least two superimposed but well-resolved pairs of the cross-peaks are clearly detected at [2.0; 0.92] MHz ($^{15}N_p$) and [1.7; 1.2] MHz ($^{15}N_\varepsilon$) with the splittings of 1.1 and 0.5 MHz, respectively, near g_z (A). Additional contribution to the ^{15}N ESEEM amplitude in the (++) quadrant of the spectra (*e.g.*, marked with red asterisk in panel C) is evident for ^{15}N-SDX (red) [and other high-potential Rieske proteins; not shown] [18,20,21], when the stacked spectra (with zero projection angles) were re-scaled and superimposed after normalizing the relative scales of the cross-peak intensities from two N_δ ligands in the (+−) quadrant (B–D). The same small τ-value (τ=136 ns; slightly exceeding the dead time of the instrument) was chosen for the measurement of these ^{15}N HYSCORE spectra, which allows the preferable observation of the undistorted lineshape of the cross-peaks as well as the minimization of the suppression effect on the ESEEM amplitudes [34]. Magnetic field, and microwave frequency, respectively: 342.5 mT (^{15}N-ARF) and 344.3 mT (^{15}N-SDX) (near g_z), 9.695 GHz (A,B); 363.1 mT (^{15}N-ARF) and 361.6 mT (^{15}N-SDX) (near g_y), 9.695 GHz (C); 387.0 mT (^{15}N-ARF) and 386.0 mT (^{15}N-SDX) (near g_x), 9.695 GHz (D).

Table 1

Isotropic and anisotropic parts of HF tensors for strongly coupled histidine $^{15}N_{\delta}$ ligands detected in the (+−) quadrant, and HF couplings of weakly coupled ^{15}N nuclei currently resolved in the (++) quadrant of ^{15}N HYSCORE spectra of the selected Rieske-type proteins

Parameters	**ARF**		**SDX**		***Rhodobacter sphaeroides* Rieske protein fragment**	
(+−) quadrant	$N_{\delta}1^{a}$ (His44)^{b}	$N_{\delta}2^{a}$ (His64)^{b}	$N_{\delta}1^{a}$ (His44)^{b}	$N_{\delta}2^{a}$ (His64)^{b}	$N_{\delta}1^{a}$ (His131)^{b}	$N_{\delta}2^{a}$ (His152)^{b}
Q	2.44	2.07	2.64	2.11	2.40	2.13
G, MHz^2	13.7	16.2	13.3	16.3	13.8	15.8
a, MHz	6.5	7.9	6.0	7.8	6.6	7.6
T, MHz	1.5	1.6	1.2	1.3	1.6	1.5
(++) quadrant^{c,d}						
g_z, MHz	0.43; 1.03^{e}		0.3; 1.03^{e}		0.36; 1.13^{e}	
g_x, MHz	0.49; 1.1		0.42; 1.04		0.43; 1.22	
g_y, MHz^{d}	0.25; 1.22		0.31; n.r.^{f}		n.r.^{f}; 1.01	
references	this work		[18]		[21]	

^{a}The terminology for $^{15}N\delta1,2$ is based on Ref. [18].

^{b}In *R. sphaeroides* cytochrome *bc1* complex, the isotropic HF constant of one of two histidine $^{14}N_{\delta}$ ligands ($^{14}a_{iso}$ ~5MHz; equivalent to $^{15}N\delta2$ in Table 1) in the presence of the Q_O-site occupant, stigmatellin, is different from the configurations in the presence of myxothiazol, suggesting that the Nδ2, at which the changes identified occur, likely belongs to His152 involved in the interaction with the Q_O-site occupants [28]. Tentative assignments of Nδ1,2 in Table 1 are made based on this previous observation in conjunction with the amino acid sequence homology, and should not be taken as definitive.

^{c}The positions of the peak maxima in this quadrant were determined with the accuracy ~0.03 MHz.

^{d}HYSCORE spectra recorded at the low- and high-field edges near the maximal and minimal g values give “single-crystal-like” patterns from the reduced cluster, whose g_Z and g_X axes are directed along the external magnetic field. In contrast, the resonance condition at the intermediate g_Y value is fulfilled by many different, yet well-defined orientations.

^{e}The relative ESEEM intensity of the largest coupling ~1.03 MHz in ^{15}N-ARF is only ~70% of that of the equivalent couplings in the high-potential protein homologs including SDX (see Fig. 2B).

^{f}Not resolved.